



Since January 2020 Elsevier has created a COVID-19 resource centre with free information in English and Mandarin on the novel coronavirus COVID-19. The COVID-19 resource centre is hosted on Elsevier Connect, the company's public news and information website.

Elsevier hereby grants permission to make all its COVID-19-related research that is available on the COVID-19 resource centre - including this research content - immediately available in PubMed Central and other publicly funded repositories, such as the WHO COVID database with rights for unrestricted research re-use and analyses in any form or by any means with acknowledgement of the original source. These permissions are granted for free by Elsevier for as long as the COVID-19 resource centre remains active.

Longitudinal Lung Function Assessment of Patients Hospitalized With COVID-19 Using ^1H and ^{129}Xe Lung MRI

^{Q38} Laura C. Saunders; Guilhem J. Collier; Ho-Fung Chan; Paul J. C. Hughes; Laurie J. Smith; James Watson; James Meiring; Zoë Gabriel; Thomas Newman; Megan Plowright; Phillip Wade; James A. Eaden; S. Thomas; S. Strickland; L. Gustafsson; Jody Bray; Helen Marshall; David J. Capener; Leanne Armstrong; Jennifer Rodgers; Martin Brook; Alberto M. Biancardi; Madhwesha R. Rao; Graham Norquay; Oliver Rodgers; Ryan Munro; James E. Ball; Neil J. Stewart; Allan Lawrie; Gisli Jenkins; James Grist; Fergus Gleeson; Rolf F. Schulte; Kevin M. Johnson; Frederick J. Wilson; Anthony Cahn; Andrew J. Swift; ^{Q1 Q2} Smitha Rajaram; Gary H. Mills; Lisa Watson; Paul J. Collini; Rod Lawson; A. A. Roger Thompson; and Jim M. Wild

BACKGROUND: Microvascular abnormalities and impaired gas transfer have been observed in patients with COVID-19. The progression of pulmonary changes in these patients remains unclear.

RESEARCH QUESTION: Do patients hospitalized with COVID-19 without evidence of architectural distortion on structural imaging exhibit longitudinal improvements in lung function measured by using ^1H and ^{129}Xe MRI between 6 and 52 weeks following hospitalization?

STUDY DESIGN AND METHODS: Patients who were hospitalized with COVID-19 pneumonia underwent a pulmonary ^1H and ^{129}Xe MRI protocol at 6, 12, 25, and 51 weeks following hospital admission in a prospective cohort study between November 2020 and February 2022. The imaging protocol was as follows: ^1H ultra-short echo time, contrast-enhanced lung perfusion, ^{129}Xe ventilation, ^{129}Xe diffusion-weighted, and ^{129}Xe spectroscopic imaging of gas exchange.

RESULTS: Nine patients were recruited (age 57 ± 14 [median \pm interquartile range] years; six of nine patients were male). Patients underwent MRI at 6 (n = 9), 12 (n = 9), 25 (n = 6), and 51 (n = 8) weeks following hospital admission. Patients with signs of interstitial lung damage were excluded. At 6 weeks, patients exhibited impaired ^{129}Xe gas transfer (RBC to membrane fraction), but lung microstructure was not increased (apparent diffusion coefficient and mean acinar airway dimensions). Minor ventilation abnormalities present in four patients were largely resolved in the 6- to 25-week period. At 12 weeks, all patients with lung perfusion data (n = 6) showed an increase in both pulmonary blood volume and flow compared with 6 weeks, although this was not statistically significant. At 12 weeks, significant improvements in ^{129}Xe gas transfer were observed compared with 6-week examinations; however, ^{129}Xe gas transfer remained abnormally low at weeks 12, 25, and 51.

INTERPRETATION: ^{129}Xe gas transfer was impaired up to 1 year following hospitalization in patients who were hospitalized with COVID-19 pneumonia, without evidence of architectural distortion on structural imaging, whereas lung ventilation was normal at 52 weeks.

CHEST 2023; ■(■):■-■

KEY WORDS: ^{129}Xe ; COVID-19; gas transfer; hyperpolarized gas; imaging; MRI; xenon MRI

ABBREVIATIONS: ADC = apparent diffusion coefficient; DCE = dynamic contrast enhanced; DW-MRI = diffusion-weighted MRI; IQR = interquartile range; Lm_D = mean acinar airway dimensions; M = membrane; M:gas = membrane to gas fraction; PFT = pulmonary function test; RBC:gas = RBC to gas fraction; RBC:M = RBC to membrane fraction; SPGR = spoiled gradient recalled; T_2^* = transverse

relaxation time; TL_{CO} = gas transfer test; UTE = ultra-short echo time; VDP = ventilation defect percentage; VP = ventilation percentage

AFFILIATIONS: From the Department of Infection, Immunity and Cardiovascular Disease (L. C. S., G. J. C., H.-F. C., P. J. C. H., L. J. S., J. A. E., S. T., J. B., H. M., D. J. C., L. A., J. R., M. B., A. M. B., M. R. R., G.

Take-home Points

Study Question: Do patients hospitalized due to COVID-19 with no evidence of architectural distortion exhibit longitudinal improvements in ^{129}Xe gas transfer (RBC:M), to within a normal range, between 6 and 52 weeks following hospitalization?

Results: At 12 weeks, significant improvements in ^{129}Xe gas transfer were observed compared with 6-week examinations. However, ^{129}Xe gas transfer remained abnormally low at weeks 12, 25, and 51.

Interpretation: In a cohort of patients with moderate severity disease, ^{129}Xe gas transfer improved but did not return to within a normal range within 1 year following hospitalization.

In patients hospitalized with pneumonia caused by infection with SARS-CoV-2, the existing literature and clinical experience suggest that there is considerable overlap in clinical presentation with typical pneumonia and ARDS, with patients exhibiting hyperinflammation and progressive hypoxemia. However, patients with severe COVID-19 also display evidence of an inflammatory and thrombotic vasculopathy with endothelial dysfunction and excessive blood flow to collapsed lung tissue.¹⁻³ Abnormal pulmonary vasoregulation has been observed in patients in the acute phase of COVID-19¹ and may be a pathophysiological mechanism contributing to the progressive hypoxemia seen in these patients.

Abnormalities on chest radiograph or CT scan imaging at 12 weeks following hospitalization due to COVID-19

N., O. R., R. M., J. E. B., N. J. S., A. L., A. J. S., G. H. M., P. J. C., A. A. R. T., and J. M. W.), University of Sheffield, Sheffield, England; Sheffield Teaching Hospitals (J. W., J. M., Z. G., T. N., M. Pl., P. W., S. S., L. G., S. R., L. W., and R. L.), NHS Foundation TRUST, Sheffield, England; National Heart and Lung Institute (A. L. and G. J.), Imperial College London, London, England; Department of Radiology (J. G. and F. G.), Oxford NHS Foundation Trust, Oxford, England; GE Healthcare (R. F. S.), Munich, Germany; University of Madison (K. M. J.), Madison, WI; and GSK (F. J. W. and A. C.), Stevenage, England.

ISMRM, 12-20.05.2021, online. "Imaging lung structure and function in acute COVID-19 patients with ^{129}Xe and ^1H MRI." ISMRM, 07-12.05.2022, London. "Longitudinal lung function assessment of patients hospitalised with COVID-19 using ^1H and ^{129}Xe lung MRI." ERS, 04-06.09.2022, Barcelona. "Longitudinal ^{129}Xe and ^1H lung MRI assessment of patients hospitalised with COVID-19."

CORRESPONDENCE TO: Jim M. Wild; email: j.m.wild@sheffield.ac.uk

Copyright © 2023 The Author(s). Published by Elsevier Inc under license from the American College of Chest Physicians. This is an open access article under the CC BY-NC-ND license (<http://creativecommons.org/licenses/by-nc-nd/4.0/>).

DOI: <https://doi.org/10.1016/j.chest.2023.03.024>

are present in some patients, particularly those with more severe disease who require ICU treatment.⁴ However, for patients without radiographic abnormalities, sensitive techniques for monitoring longitudinal change in lung function are needed.

Lung MRI with hyperpolarized ^{129}Xe gas allows direct, regionally sensitive measurements of lung ventilation and function, and it is an emerging method that is used both clinically and in clinical research, alongside ^1H MRI, to evaluate lung function and abnormalities.⁵⁻¹¹ In addition, ^{129}Xe can image gas diffusion within the lung airspace (diffusion-weighted MRI [DW-MRI]), and the derived apparent diffusion coefficient (ADC) and mean acinar airway dimensions (L_{mD}) provide three-dimensional in vivo information of the underlying lung microstructure that is highly sensitive to changes in lung microstructure in patients with emphysema¹² and fibrotic lung disease.¹³ In addition, ^{129}Xe is soluble in the interstitium/membrane (M) and in the RBCs, and the signal from ^{129}Xe in these dissolved compartments can be distinguished spectroscopically. The ratio of the ^{129}Xe MRI signal observed in the lung airspaces (gas), the lung M, and bound to the RBCs can thus be determined with magnetic resonance spectroscopic imaging. In particular, the fractions of the ^{129}Xe signal in the RBC:M, RBC:gas, and M:gas ratios have been used to probe gas transfer^{14,15} and are highly sensitive to gas transfer limitation and longitudinal change in interstitial, emphysematous, and pulmonary vascular diseases.¹⁶⁻¹⁸ RBC:M has been shown to correlate highly with the gas transfer test (TL_{CO}).^{6,19}

Previous studies have reported reduced RBC:M in patients with COVID-19,²⁰⁻²³ including in patients with normal chest CT scan imaging but ongoing dyspnea.²¹ In patients with residual lung abnormalities on CT scans, decreased RBC:M may be due to an increase of xenon uptake in the interstitial lung tissue. However, in the absence of CT scan abnormalities, we propose that a decreased RBC:M instead indicates microvascular (capillary) abnormalities. Therefore, RBC:M in particular may be a sensitive metric suitable for longitudinal assessment of regional gas exchange abnormalities in patients who have had COVID-19 and have normal structural imaging. It is currently unknown whether RBC:M improves longitudinally following COVID-19 pneumonia. Age-related reductions in the RBC:M ratio may be relevant in other cohorts,²⁴ and control cohorts well-matched for age are therefore needed for accurate interpretation of RBC:M in post-COVID-19 studies. It is also unclear whether patients

with abnormal RBC:M have concurrent abnormalities in lung perfusion or ventilation.

^1H lung MRI is able to assess changes in lung structure and perfusion. Ultra-short echo time (UTE) imaging enables good visualization of the lung parenchyma and has shown excellent agreement with CT scan imaging in the visualization of lesions in patients with COVID-19.²⁵ Dynamic contrast-enhanced (DCE) ^1H lung MRI allows the assessment of lung perfusion, with high sensitivity and specificity in detecting perfusion defects without exposing the participant to ionizing radiation,²⁶ and it is therefore well suited for patient follow-up studies. Increased lung perfusion transit times (time to peak) have been reported in both an acute hospitalized patient with COVID-19 and in nonhospitalized male patients with breathlessness who have had COVID-19.^{27,28}

Study Design and Methods

Participants

Patients with acute COVID-19 pneumonia and no previously diagnosed respiratory disease (excluding mild asthma) were recruited from [institution name removed] pulmonology and infectious diseases wards from November 2020 to February 2022 for this prospective cohort study, prior to or shortly following discharge. Follow-up ^{129}Xe and ^1H lung MRI examinations were acquired at approximately 6, 12, 24, and 52 weeks following COVID-19 infection. Patients were required to meet the following criteria: (1) a positive SARS-CoV-2 result from a nasal/pharyngeal or respiratory sample; (2) hospitalization with a diagnosis of pneumonia (chest radiograph or CT scan consistent with COVID-19 infection); (3) development of impaired oxygenation (pulse oximetry saturation $\leq 93\%$ on room air) requiring additional oxygen; and (4) no evidence of interstitial lung damage on CT scan or MRI structural imaging at 12 weeks following hospital admission, as judged by a clinical chest radiologist.

Patients with evidence of interstitial lung damage at 12 weeks following hospital admission were recruited into the parallel UK Interstitial Lung Disease Consortium (UKILD) study.²⁹ Standard MRI exclusion criteria were applied to all subjects. In addition, patients were excluded if they were unable to tolerate a test inhalation of ^{129}Xe gas according to the supervising clinicians' judgment or if they had a chest size exceeding the ^{129}Xe chest coil circumference (76 cm).

Where possible, PFTs were acquired on the same day as the MRI examination at each visit. Spirometry and transfer factor were performed, and from these tests, the metrics FEV₁, FVC, FEV₁/FVC, TL_{CO}, and carbon monoxide transfer coefficient were calculated and presented as z scores and % predicted using Global Lung Function Initiative reference ranges.^{30,31} This study was approved by the London-Hampstead Research Ethics Committee (REC reference: 9/LO/1115).

MRI Acquisition

Patients underwent scanning on either an HDx 1.5T (N = 7) or a 450w 1.5T (N = 2) (GE Healthcare) MRI scanner.³² The ^{129}Xe images were acquired with the patient in a flexible quadrature transmit/receive vest coil (Clinical MR Solutions). Patients' vital signs were monitored throughout the MRI examination. Each patient underwent MRI

The current study used a ^1H and ^{129}Xe MRI protocol that combines hyperpolarized ^{129}Xe imaging methods sensitive to ventilation, lung microstructure (DW-MRI), and gas exchange (dissolved xenon spectroscopic imaging) alongside ^1H DCE perfusion and UTE lung structural imaging to assess pathophysiological changes in patients who had been hospitalized with COVID-19 pneumonia, during the postacute period. The primary hypothesis of this work was that abnormal imaging and pulmonary function test (PFT) markers of lung function would increase to within a normal range over the course of 1 year in patients without structural abnormalities seen on CT scan or proton structural imaging. Patients underwent up to four follow-up MRI examinations at approximately 6, 12, 24, and 52 weeks following hospitalization.

examinations on the same scanner for baseline visits and follow-up. Figure 1 presents an illustrative diagram of the lung MRI methods used in this study.

^{129}Xe doses were polarized to approximately 30% using a home-built high-performance spin-exchange optical pumping polarizer.³² This had regulatory approval for manufacture of hyperpolarized ^{129}Xe for clinical lung MRI by the UK Medicines and Healthcare Products Regulatory Agency.

MR imaging was conducted as summarized in the following text (parameters are detailed in e-Table 1).

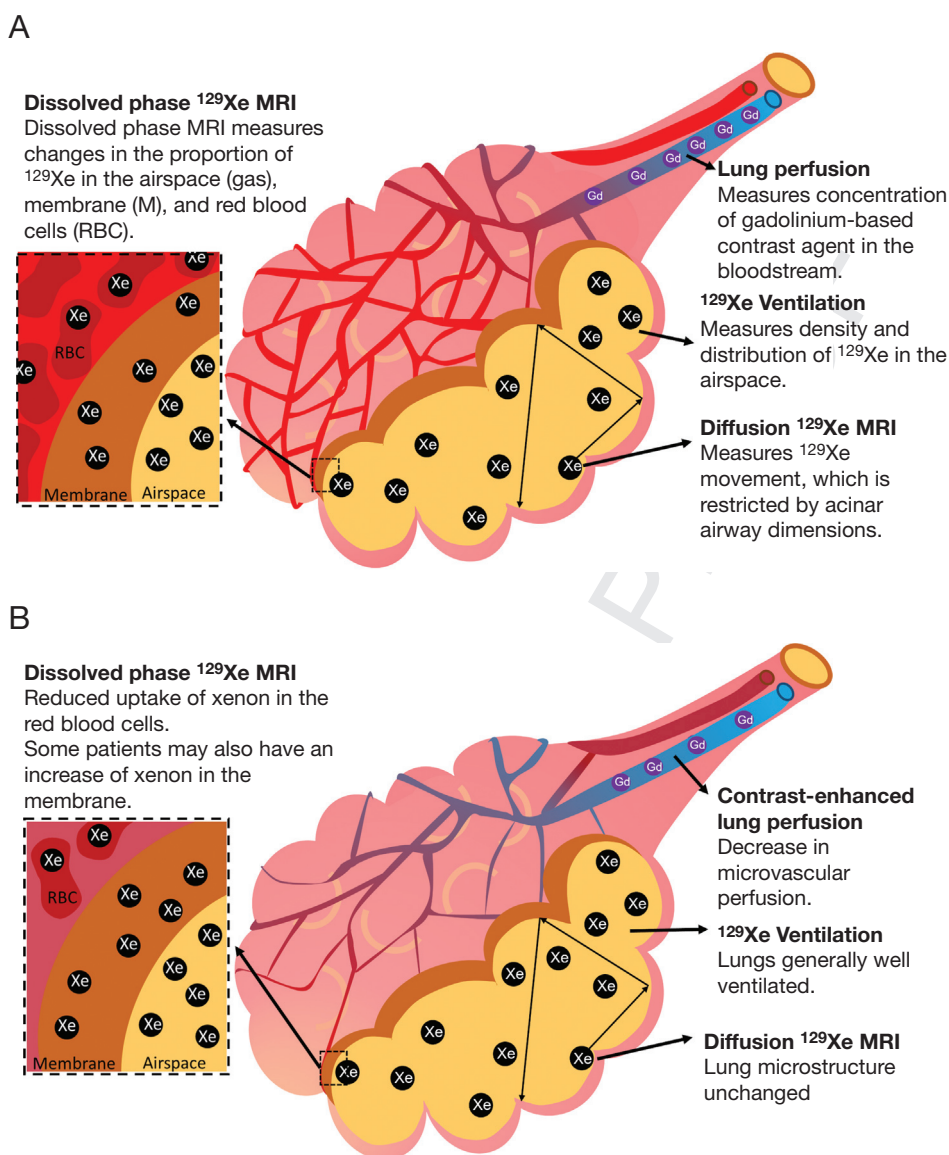
A structural ^1H scan was acquired following inhalation of a bag of air to match the lung inflation state of the subsequent xenon sequences. ^{129}Xe ventilation images were acquired using a three-dimensional imaging sequence with whole-lung coverage following inhalation of a 1 L maximum mixture of ^{129}Xe and N_2 (titrated if subject height < 160 cm³³) and inhaled from functional residual capacity; patients were coached in the required breathing maneuver prior to their MRI examination.³⁴

^{129}Xe DW-MRI to assess alveolar microstructural change was acquired following inhalation of a maximum 1 L mixture of ^{129}Xe and N_2 (three-dimensional spoiled gradient echo [SPGR] multiple b-value sequence with compressed sensing with whole-lung coverage).³⁵

Three-dimensional spectroscopic imaging of the gas and dissolved phase xenon resonances (dissolved xenon in lung M and in blood RBCs) was acquired by using a maximum 1 L dose of hyperpolarized ^{129}Xe (TR = 15, flip angle = 22 [three-dimensional acquisition with whole-lung coverage]).⁵

^1H MRI was acquired by using an eight-element cardiac array (GE Healthcare). UTE images were acquired with a three-dimensional radial sequence during 8 min of free-breathing with prospective respiratory bellows gating on expiration.³⁶

Three-dimensional variable flip angle SPGR images^{37,38} were acquired (flip angle = 2°, 4°, 10°, and 30°) to allow for the correction of lung T₁ and proton density. DCE lung perfusion MRI was acquired (three-dimensional volumetric time-resolved SPGR acquisition). A half dose (0.05 mL/kg) of Gadovist (Bayer) was administered at an injection rate of 4 mL/s followed by a 20 mL saline flush at 4 mL/s. Patients



369 Figure 1 – A-B, Illustrative diagram showing how the lung MRI techniques used in this article measure lung perfusion, ventilation, lung microstructure (acinar airway dimensions), and xenon gas transfer (the transfer of xenon between the airspace, membrane, and RBCs). A, Techniques in a healthy alveolus. B, Possible interpretation of the findings of this article in patients who have had COVID-19, with reduced RBC:M due to damage to pulmonary microcirculation but preserved acinar airway dimensions.

were advised to hold their breath for as long as possible and breathe shallowly thereafter.

Image Analysis

Qualitative assessments of the UTE ^1H structural, ^{129}Xe ventilation, and DCE lung perfusion images were made by two radiologists with 10 and 14 years of experience, respectively. UTE images were assessed for parenchymal changes, and ventilation and perfusion images were assessed for defects.

Metrics of ventilation defect percentage (VDP), low ventilation percentage (VP), normal VP, and hyper VP for each patient were calculated by using linear binning (see [online supplement](#)). The coefficient of variation of the segmented lung ventilation images was also calculated from the ^{129}Xe ventilation images as a marker of ventilation heterogeneity.

Maps of ^{129}Xe ADC and mean diffusive length scale (L_{mD}) from a stretched exponential model of ^{129}Xe gas diffusion in the lungs were calculated on a voxel-by-voxel basis.³⁹

Maps of gas transfer ratios (RBC:M, RBC:gas, and M:gas) were calculated from three-dimensional spectroscopic imaging. The transverse relaxation time (T_2^*) of the RBC and M spectroscopic peaks was also calculated.

Mean values of all global metrics were calculated for each patient. A sample size calculation was not performed because this was an exploratory study.

Global MRI metrics from visits 1, 2, 3, and 4 were compared by using a Skillings-Mack test due to the presence of missing data⁴⁰ with pairwise Wilcoxon tests and a correction for multiple testing,⁴¹ implemented by using R software.⁴² Data are presented as median (range), unless otherwise stated.

Mixed linear effect models were set up using a random intercept model to test the relationship between RBC:M and the following: (1) pulmonary blood volume; (2) pulmonary blood flow; (3) mean transit time; (4) VDP; and (5) TL_{CO} z score. IBM SPSS Statistics 27 (IBM SPSS Statistics, IBM Corporation) was used for analysis. A *P* value < .05 was considered statistically significant.

Age- and Sex-Matched Healthy Volunteer Metrics

Median ADC and Lm_D values for an age- and sex-matched control cohort were determined by retrospective analysis of previously published data.⁴³ Eleven subjects from this previously published

work were selected based on matching median and interquartile range (IQR) of age and sex ratio from a cohort of 23 subjects while blinded to MRI metrics; the control cohort had a median age of 63 (40-70) years, and 73% were male.

Median RBC:M, RBC:gas, and M:gas for an age- and sex-matched control cohort were determined by retrospective analysis of a healthy cohort data set, with control subjects chosen based on matching median and IQR of age and sex ratio while blinded to MRI metrics. Twelve subjects were selected (median age, 57 [41-68] years), and 67% were male.

Results

Of the 16 recruited patients, 14 showed no signs of interstitial lung damage at 12 weeks and were therefore included as part of this study. Nine of 14 patients had follow-up examinations and were included for analysis (Fig 2).

Six of nine patients were male. Median patient age, height, and weight were 57 (42-72) years, 173 (170-191) cm, and 101 (84-112) kg, respectively. Visit 1 (*N* = 9) occurred 6 (4-12) weeks following hospital admission; visit 2 (*N* = 9) occurred 12 (11-22) weeks following hospital admission; visit 3 (*n* = 7) occurred 25 (23-28) weeks following hospital admission; and visit 4 (*n* = 8) occurred 51 (49-62) weeks following hospital admission. Patients had been admitted to the

hospital with COVID-19 for 6 (2-15) days. Further patient demographic data are presented in Table 1.^{44,45} No patients received any trial of pharmacologic treatment for post-COVID-19 symptoms following discharge. Two of the patients commenced treatment for diabetes during the follow-up period.

UTE and ^{129}Xe MRI were successfully acquired in all patients at all visits. DCE lung perfusion imaging was successfully acquired in six of nine patients at visit 1, eight of nine patients at visit 2, six of seven patients at visit 3, and five of eight patients at visit 4. The reasons for unsuccessful lung perfusion imaging were patients failing screening (6 visits), patient motion (2 visits), and technical issues (1 visit).

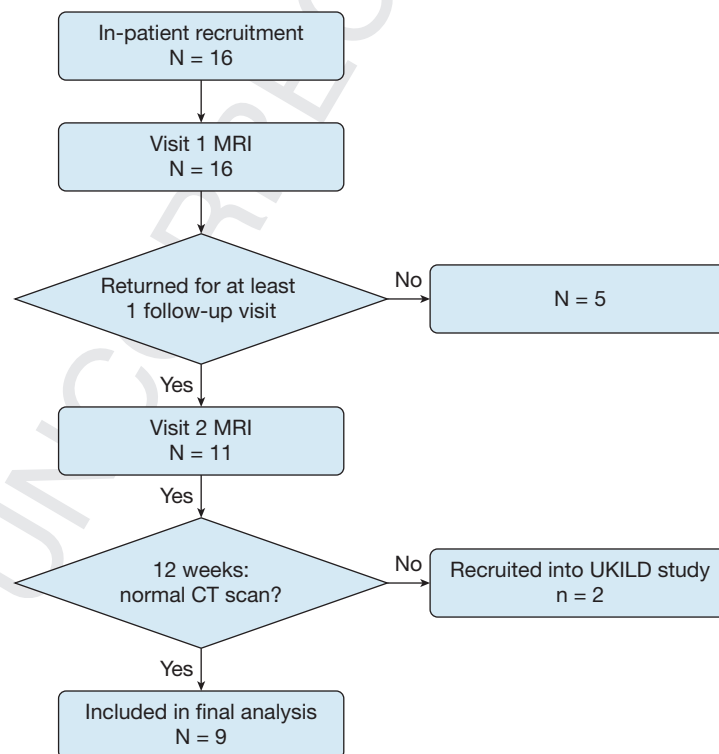


Figure 2 – Flow chart of patient recruitment. UKILD = UK Interstitial Lung Disease Consortium.

551 Q27 TABLE 1] Patient Demographic Data

Characteristic	Group	No. of Patients
Demographic characteristics		
Age, y	< 50	2
	50-59	3
	60-69	3
	70-79	1
Sex	Male	6
	Female	3
BMI, kg/m ²	25-29.9	3
	30-39.9	5
	≥ 40	1
	Comorbidities 4C score ⁴⁴	0
	1	4
	3	1
Tobacco use history	Never tobacco user	4
	Ex-tobacco user	5
Clinical characteristics on admission		
Admission SF ratio	< 200	0
	200-299	3
	300-399	3
	≥ 400	3
Clinical characteristics during admission		
Maximum oxygen requirement during hospital stay	< 28%	1
	28%-35%	4
	40%	2
	> 60%	2
	CPAP	1
	ISARIC 4C score ⁴⁴	1-4
	5-8	5
	> 8	1
Length of stay, d	1-5	4
	6-9	4
	> 10	1
Maximum National Early Warning Score 2 score ⁴⁵	5-6	4
	≥ 7	5
Medication during stay	Oral antibiotics	1
	IV antibiotics	2

(Continued)

TABLE 1] (Continued)

Characteristic	Group	No. of Patients
	Dexamethasone	9
	Remdesivir (Gilead Sciences)	5
	Immunomodulation therapy	3
	Convalescent plasma	2
	Colchicine	2
	Aspirin	3
	Included in an interventional study?	7
Lowest SF ratio during stay	< 200	2
	200-299	3
	300-399	4
	≥ 400	0
Maximum Fio ₂ during stay	< 28%	1
	28%-35%	4
	40%	2
	> 60%	2
	CPAP	1
Clinical characteristics postdischarge		
MRC Dyspnoea Scale (1-5), 6 wk	1	6
	2	2
	Not available	1
MRC Dyspnoea Scale (1-5), 3 mo	1	7
	2	1
	3	1
	Not available	0
Readmittance	Yes	1 for general surgery unrelated to COVID-19
	No	8

Ex-tobacco users all reported ≤ 15 pack y. The pulse oximetry saturation/Fio₂ ratio (SF ratio) was calculated by using estimated Fio₂ based on flow rate when delivered by nasal cannulae. ISARIC = International Severe Acute Respiratory and Emerging Infection Consortium; MRC = Medical Research Council.

Figure 3 shows representative slices from the UTE images, RBC:M maps, ¹²⁹Xe ventilation images, and DCE pulmonary blood flow maps for each patient at

661
662
663
664
665
666
667
668
669
670
671
672
673
674
675
676
677
678
679
680
681
682
683
684
685
686
687
688
689
690
691
692
693
694
695
696
697
698
699
700
701
702
703
704
705
706
707
708
709
710
711
712
713
714
715

print & web 4C/FPO

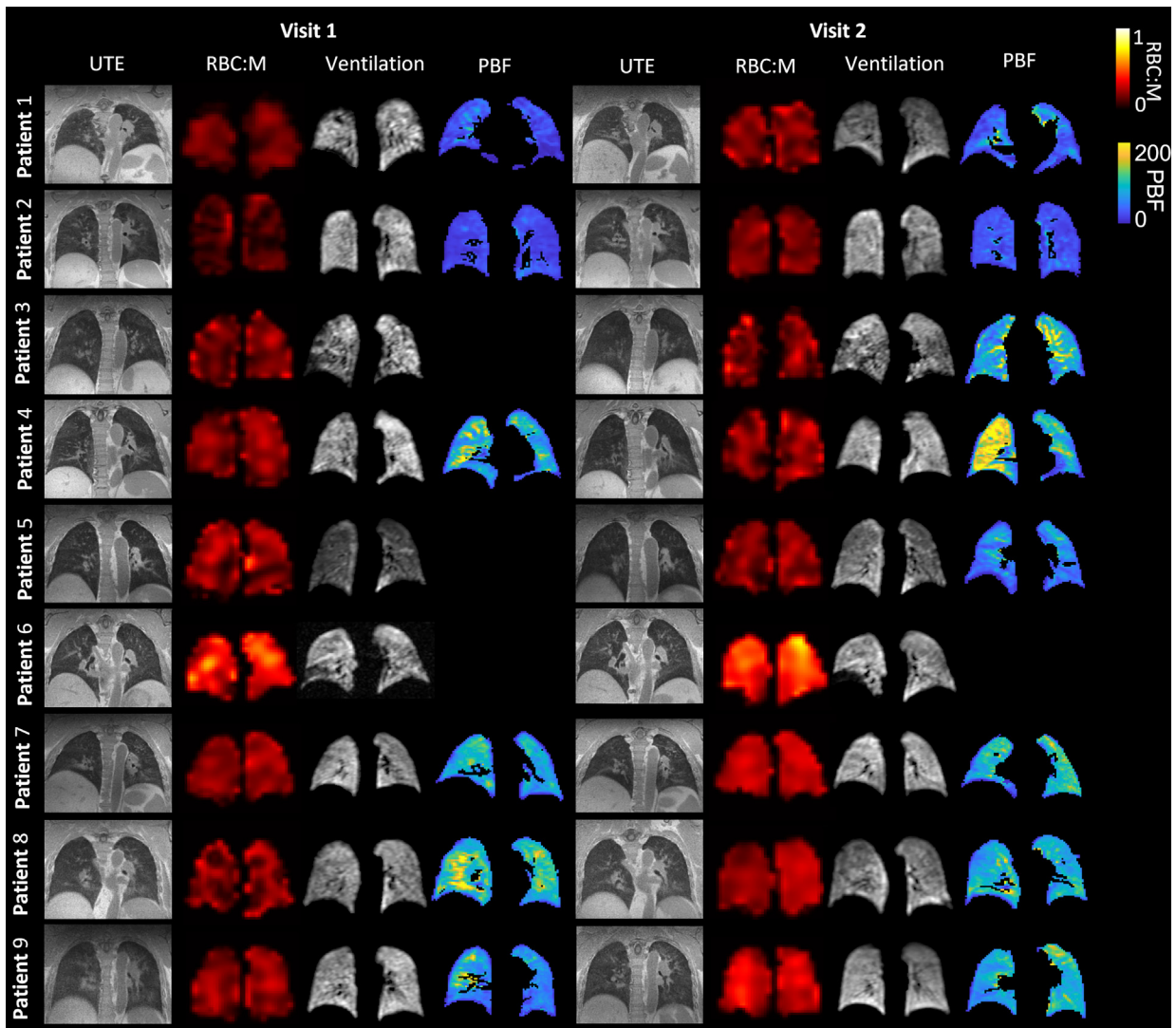
716
717
718
719
720
721
722
723
724
725
726
727
728
729
730
731
732
733
734
735
736
737
738
739
740
741
742
743
744
745
746
747
748
749
750
751
752
753
754
755
756
757
758
759
760
761
762
763
764
765
766
767
768
769
770

Figure 3 – Example of UTE images, RBC:M maps, ^{129}Xe ventilation images, and maps of pulmonary blood flow at visit 1 and visit 2, for each patient. The white arrow indicates a segmental perfusion defect visible at visit 1, which improves at visit 2. M = membrane; PBF = pulmonary blood flow; UTE = ultra-short echo time.

visit 1 and visit 2. Figure 4 displays plots of ventilation, dissolved phase ^{129}Xe , and DCE lung perfusion metrics for each patient at each visit. Median metrics and statistical comparisons of metrics at each visit are presented in Table 2.

^{129}Xe MRI

Ventilation: At visit 1, small ventilation defects were visible in the lung periphery in four patients (1, 3, 4, and 6). No other patients had visible lung ventilation defects. At visits 2 and 3, the ventilation defects observed in patients 1, 3, 4, and 6 had improved, with small defects still visible, particularly in patient 3. At visit 4, small peripheral ventilation defects were observed in patients 1, 3, and 6 (e-Fig 1, Fig 3).

Whole lung VDP was calculated for each patient. At visit 1, median VDP was 1.6% (0.6%-3.9%); at visit 2, VDP was 1.3% (0.7%-2.6%); at visit 3, VDP was 1.2% (0.4%-2.1%); and at visit 4, VDP was 0.8 % (0.4%-3.7%).

Quantitative metrics of ventilation improved at visits 2, 3, and 4 compared with visit 1; however, this was not statistically significant following adjustment for multiple corrections (Table 2).

DW-MRI (Alveolar Microstructure): Median ADC and Lm_D at each visit are reported in Table 2. No significant longitudinal changes in ADC and Lm_D were seen between visits. Median ADC and Lm_D were within the median \pm IQR of age- and sex-matched control data (age- and sex-matched control data: median ADC,

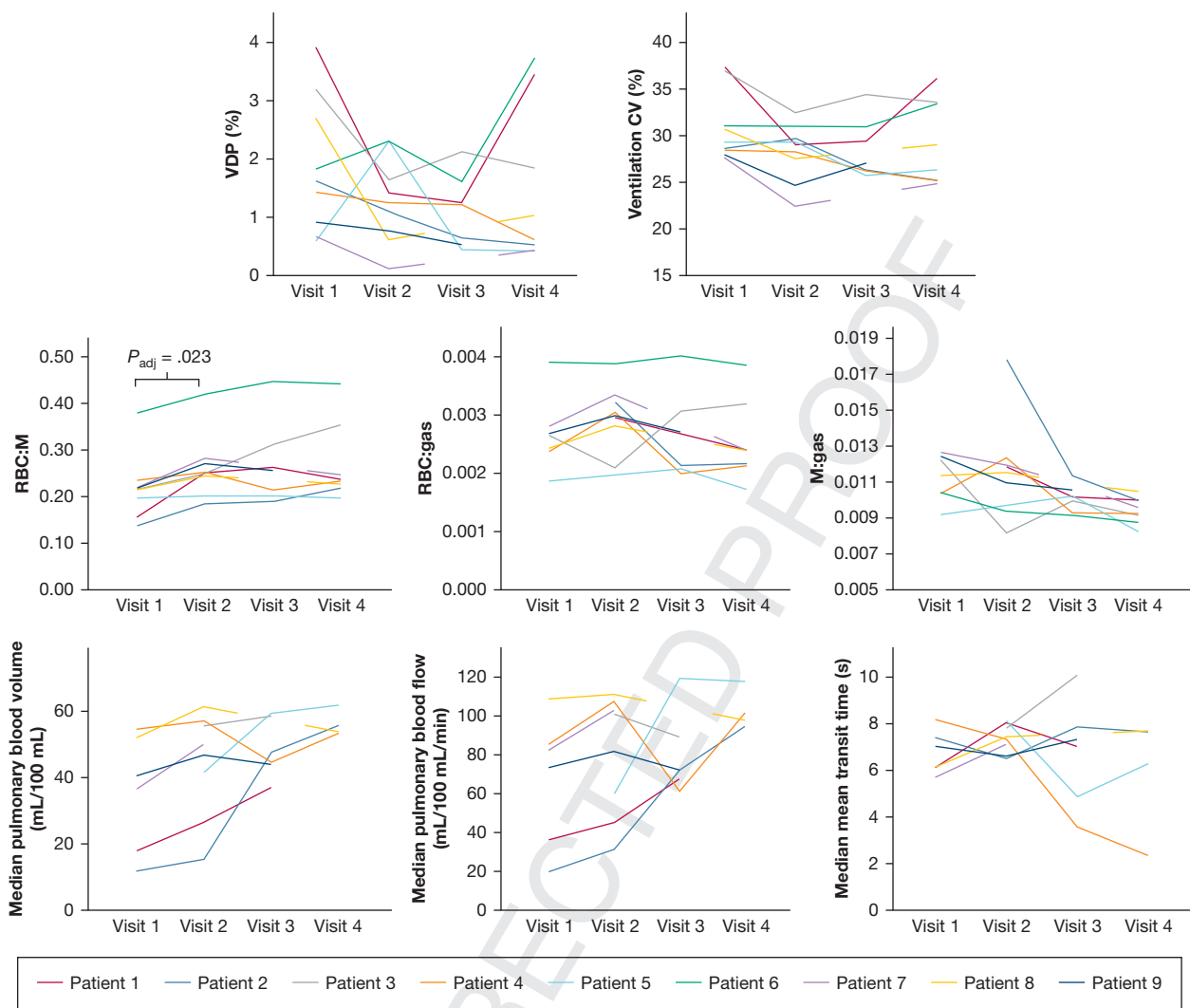


Figure 4 – Spaghetti plots of ventilation, dissolved phase xenon, and dynamic contrast-enhanced lung perfusion metrics at visits 1 to 4. CV = coefficient of variation of lung ventilation; M = membrane; VDP = ventilation defect percentage.

0.0360 cm²/s [IQR, 0.005 cm²/s]; median Lm_D, 289 μm [IQR, 27 μm]) at all visits (e-Fig 2).

Dissolved Xenon (Gas Exchange): Figure 5 presents sample RBC:M maps. The global RBC:M ratio significantly increased at visit 2 compared with visit 1 ($P_{\text{adj}} = .023$). RBC:M at visit 1 was 0.22 (0.15-0.37), and at visit 2 it was 0.25 (0.18-0.41). No subjects showed a decrease in RBC:M at visit 2 compared with visit 1 (Figs 4, 5). RBC:M at visits 3 and 4 were 0.25 (0.19-0.44) and 0.23 (0.19-0.44), respectively. At visits 3 and 4, some patients showed continued improvement (Figs 3, 4), while others maintained an abnormal RBC:M during the 25- to 51-week period. There were no significant changes between visits 2, 3, and 4.

Figure 6 shows boxplots of the RBC:M, RBC:gas, and M:gas for patients at each visit, with reference boxplots of age- and sex-matched control data (control RBC:M median, 0.39 [IQR, 0.13]; RBC:gas median, 0.0034 [IQR, 0.0006]; M:gas median, 0.0088 [IQR, 0.0021]). The number of patients who had RBC:M below the median ± IQR of the age- and sex-matched healthy volunteers was eight of nine at visit 1, seven of nine at visit 2, five of seven at visit 3, and six of eight at visit 4.

The T_2^* of the M and RBCs was calculated. M T_2^* showed a significant longitudinal decrease across visits, with lower M T_2^* at visit 4 compared with visits 1, 2, and 3 ($P_{\text{adj}} = .023$, $P_{\text{adj}} = .023$, and $P_{\text{adj}} = .047$, respectively) and between visits 1 and 3 ($P_{\text{adj}} = .031$) (Table 2). No

881
882
883
884
885
886
887
888
889
890
891
892
893
894
895
896
897
898
899
900
901
902
903
904
905
906
907
908
909
910
911
912
913
914
915
916
917
918
919
920
921
922
923
924
925
926
927
928
929
930
931
932
933
934
935

TABLE 2] Median Metrics for All MRI Parameters at Visits 1, 2, 3, and 4

	Visit 1	Visit 2	Visit 3	Visit 4	P Value	Adjusted P Value
No.	9	9	7	8		
ADC, cm ² /s	0.0344 (0.309-0.0373)	0.0327 (0.0281-0.0386)	0.0340 (0.310-0.364)	0.0338 (0.307-0.0357)
Lm _D , μm	281 (260-300)	273 (251-301)	278 (263-290)	279 (263-288)
RBC:M	0.22 (0.15-0.37)	0.25 (0.18-0.41)	0.25 (0.19-0.44)	0.23 (0.19-0.44)	V1-V2, P = .004 V1-V3, P = .047 V1-V4, P = .039	V1-V2, P = .023* V1-V3, P = .094 V1, V4, P = .094
RBC:gas	0.0026 (0.0018-0.0039)	0.0030 (0.0019-0.0038)	0.0026 (0.0020-0.0040)	0.0024 (0.0017-0.0038)
M:gas	0.0113 (0.0091-0.0125)	0.0114 (0.0081-0.0179)	0.0101 (0.0091-0.0113)	0.0094 (0.0082-0.0104)	V1-V4, P = .031 V2-V4, P = .023 V3-V4, P = .031	V1-V4, P = .063 V2-V4, P = .063 V3-V4, P = .063
M T ₂ [*] , ms	2.58 (2.46-2.68)	2.47 (2.38-2.58)	2.42 (2.36-2.56)	2.22 (1.94-2.40)	V1-V2, P = .044 V1-V3, P = .023 V1-V4, P = .008 V2-V4, P = .008 V3-V4, P = .031	V1-V2, P = .053 V1-V3, P = .031* V1-V4, P = .023* V2-V4, P = .023* V3-V4, P = .047*
RBC T ₂ [*] , ms	2.20 (2.05-2.48)	2.16 (2.01-2.49)	2.16 (2.06-2.32)	2.27 (2.10-2.47)
DCE PBV, mL/ 100 mL	37.8 (11.7-53.5)	47.6 (15.0-60.2)	45.3 (36.3-58.4)	53.8 (52.46-60.72)
SD PBV, mL/ 100 mL	18.0 (7.5-28.5)	21.3 (13.0-24.8)	23.8 (17.9-25.7)	21.1 (20.8-22.0)
IQR PBV, mL/ 100 mL	25.1 (7.8-34.9)	27.8 (10.5-36.1)	35.9 (24.2-41.5)	29.5 (27.0-31.9)
DCE PBF, mL/ 100 mL/min	76.9 (19.6-107.2)	90.2 (30.7-109.5)	71.1 (60.3-117.7)	98.3 (93.4-116.2)
SD PBF, mL/ 100 mL/min	45.8 (11.5-58.8)	54.5 (32.0-75.0)	48.6 (35.6-69.5)	54.2 (41.0-65.4)
IQR PBF, mL/ 100 mL/min	54.0 (14.1-61.3)	59.2 (25.5-102.9)	59.0 (43.2-78.7)	64.8 (54.2-72.4)
Median MTT, s	6.5 (5.6-8.0)	7.3 (6.4-8.0)	7.1 (3.5-9.9)	6.9 (2.3 - 7.6)
SD MTT, s	1.3 (0.9-1.6)	1.2 (0.6-2.6)	1.3 (0.5-2.2)	0.7 (0.6-0.9)
IQR MTT, s	1.3 (1.1-2.0)	1.6 (0.7-3.1)	1.3 (0.6-3.5)	0.7 (0.5-1.1)
VDP, %	1.6 (0.6-3.9)	1.3 (0.7-2.6)	1.2 (0.4-2.1)	0.8 (0.4-3.7)	V1-V3, P = .016	V1-V3, P = .094
Normal VP, %	76.4 (62.5-77.7)	76.9 (72.3-86.2)	78.9 (67.4-81.5)	81.1 (69.0-82.6)	V1-V2, P = .027 V1-V3, P = .031	V1-V2, P = .093 V1-V3, P = .093
Low VP, %	12.5 (10.0-15.4)	11.9 (8.9-13.1)	10.9 (9.1-14.8)	10.6 (10.0-13.7)

(Continued)

Q29 Q30
Q31936
937
938
939
940
941
942
943
944
945
946
947
948
949
950
951
952
953
954
955
956
957
958
959
960
961
962
963
964
965
966
967
968
969
970
971
972
973
974
975
976
977
978
979
980
981
982
983
984
985
986
987
988
989
990

TABLE 2] (Continued)

	Visit 1	Visit 2	Visit 3	Visit 4	P Value	Adjusted P Value
Hyper VP, %	11.7 (9.5-18.3)	11.0 (4.2-13.3)	9.7 (7.9-15.8)	8.4 (6.8-15.2)
Lung ventilation CV, %	29.0 (27.5-37.1)	28.8 (22.3-32.2)	26.9 (25.6-34.1)	26.1 (25.0-33.3)	V1-V2, P = .040 V1-V3, P = .016 V1-V4, P = .040	V1-V2, P = .078 V1-V3, P = .078 V1-V4, P = .078

Data are presented as median (range) of all patients with available data for each visit. If a Skillings-Mack test determined that there was a significant difference between at least two variables, P values are shown for Wilcoxon pairwise tests. P values are shown prior to and following adjustment for multiple testing. ADC = apparent diffusion coefficient; CV = coefficient of variation; DCE = dynamic contrast-enhanced; IQR = interquartile range; Lm₀ = mean acinar airway dimensions; M = membrane; M₀ = membrane to gas fraction; MTT = mean transit time; PBF = pulmonary blood flow; PBV = pulmonary blood volume; RBC:gas = RBC to gas fraction; T₂* = transverse relaxation time; V = visit; VDP = ventilation defect percentage; VP = ventilation percentage.

other significant changes in the T₂* of the RBC or M were seen (e-Fig 3).

¹H MRI

Structural Changes: The UTE image of Patient 3 showed abnormal linear parenchymal changes at visit 1, which improved but remained abnormal at visits 2 and 3 and were resolved at visit 4. Patients 2, 6, 7, and 8 displayed air trapping on their UTE image at visit 1, which resolved at visit 2 for patients 6, 7, and 8. Patient 2 continued to have air trapping present at visits 3 and 4. The UTE images of Patients 1, 4, 5, and 9 were normal at all visits (e-Table 2).

DCE (Perfusion): Patient 1 showed a segmental perfusion defect at visit 1 that was resolved at visit 2. No other patients showed any substantial regional perfusion defects. Median pulmonary blood volume and flow increased in all patients (n = 6) at visit 2 compared with visit 1; however, the increase was not statistically significant. For the six patients with DCE MRI at visits 1 and 2, median pulmonary blood volume was 37.8 (11.7-53.5) mL/100 mL at visit 1 and 47.6 (15.0-60.2) mL/100 mL at visit 2, and pulmonary blood flow was 76.9 (19.6-107.2) mL/100 mL/min at visit 1 and 91.1 (30.7-109.5) mL/100 mL/min at visit 2 (Fig 4).

Pulmonary Function Tests

Data were available on PFTs for six of nine patients at visit 1, six of nine patients at visit 2, seven of seven patients at visit 3, and seven of eight patients at visit 4; all z scores and % predicted data are shown in Figure 7. There was a median of 0 days (mean, 2.8 days; range, 0-23 days) between MRI and PFTs.

Median TL_{CO} z score was -1.66 (-1.96 to 0.66) at visit 1, -0.88 (-1.49 to 0.68) at visit 2, -0.47 (-1.51 to 0.90) at visit 3, and -0.31 (-1.67 to 1.05) at visit 4. Three of six patients had an abnormal TL_{CO} z score (<1.64) at visit 1. No patients had an abnormal TL_{CO} z score at visit 2 or 3. One patient had an abnormal TL_{CO} z score at visit 4.

One patient (patient 5) had abnormally low FVC at visit 1 and visit 4. No other forced lung volume metrics were abnormal at any visits.

Linear Mixed-Effect Model of RBC:M

A significant increase in RBC:M was found with increasing pulmonary blood volume, pulmonary blood flow, decreasing VDP, and increasing TL_{CO} z score, using data from all 4 visits (Table 3). No statistically significant relationship was found between RBC:M and mean transit time.

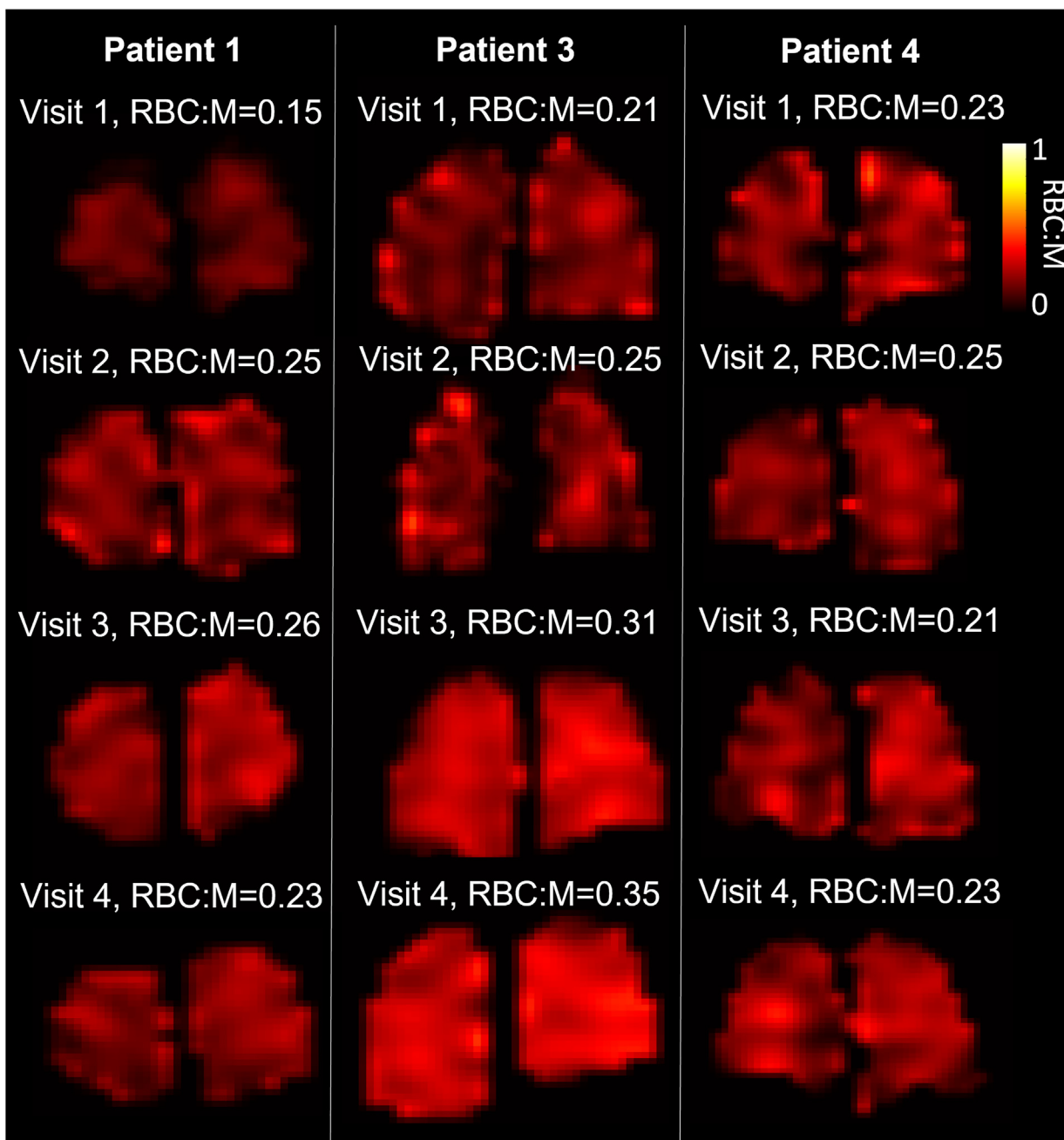


Figure 5 – Lung RBC:M maps in three patients with four MRI visits at 6, 12, 25, and 51 weeks following hospital admission. Mean RBC:M at each visit is shown. *M* = membrane.

Discussion

This study used a comprehensive ^1H and ^{129}Xe MRI protocol to assess pathophysiological pulmonary changes in hospitalized patients with COVID-19 for up to 1 year following hospitalization. At 6 weeks following hospitalization, four of nine patients had small ventilation defects, TL_{CO} *z* score was abnormal in three of nine patients, and xenon gas transfer (RBC:M) was outside the median \pm IQR of age- and sex-matched

healthy subjects in eight of nine patients. At 12 weeks, improvements were seen in lung ventilation and xenon gas transfer. However, there was no longitudinal change in xenon gas transfer between 12 and 52 weeks, and median ^{129}Xe gas transfer in these patients remained lower than expected. This indicates that some of the patients with COVID-19 exhibited continued abnormalities in ^{129}Xe gas transfer at 12 to 51 weeks following hospitalization, despite normal lung structural

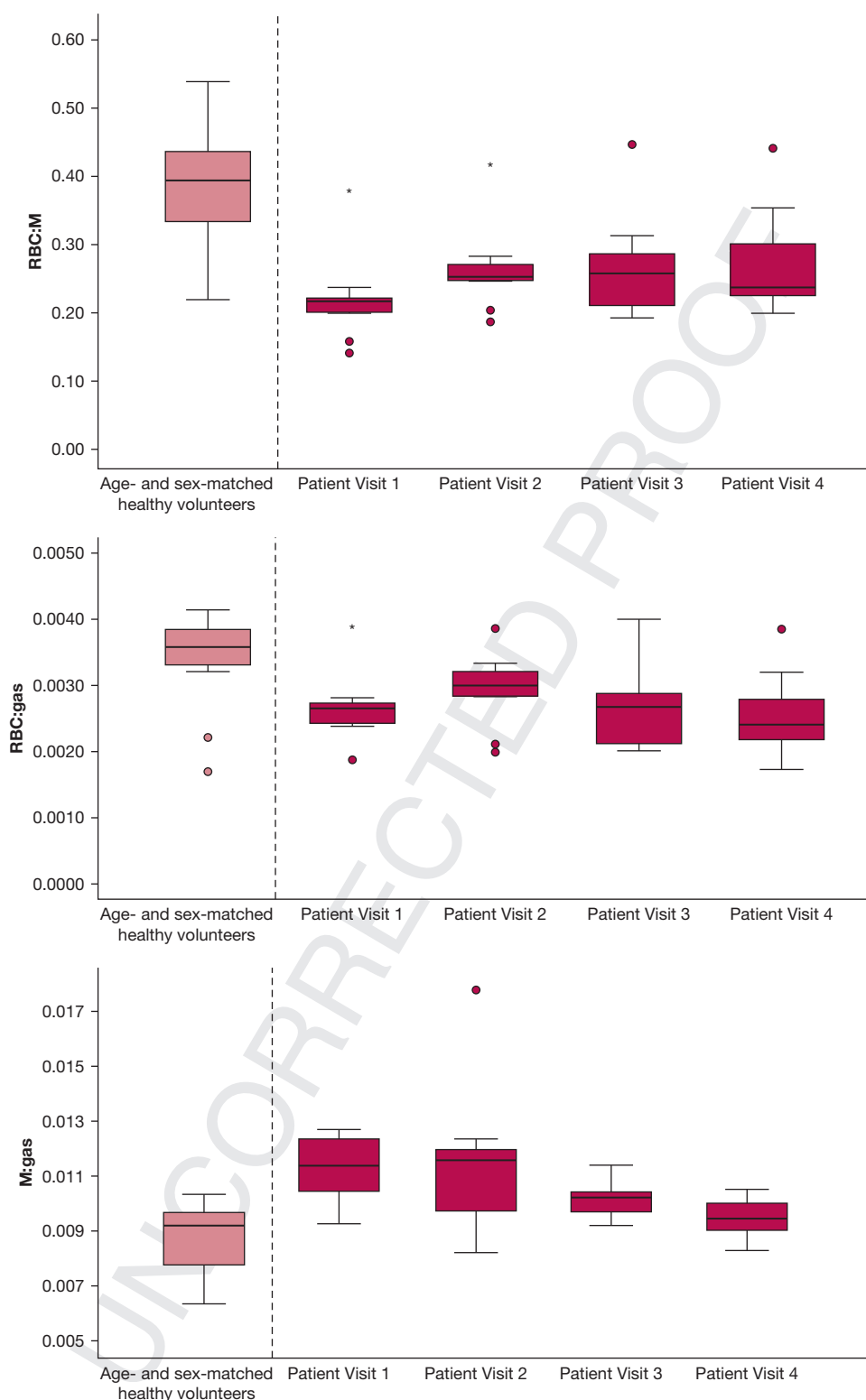
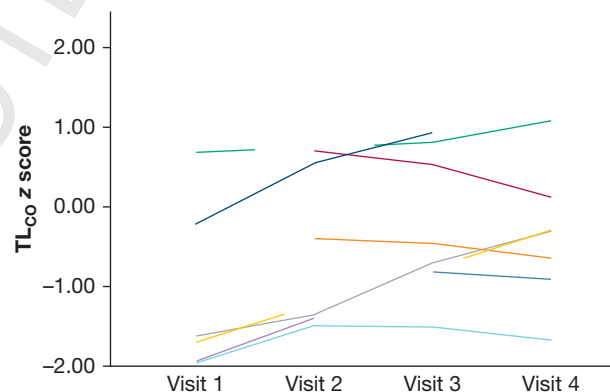
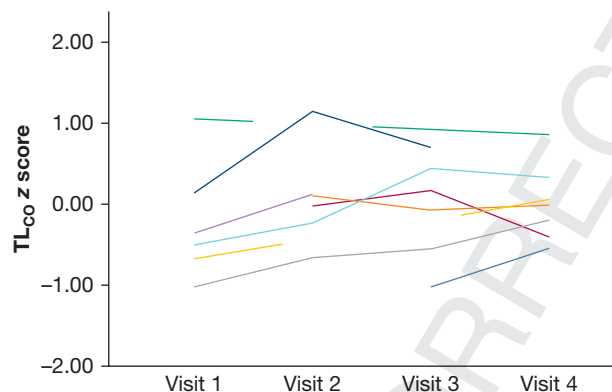
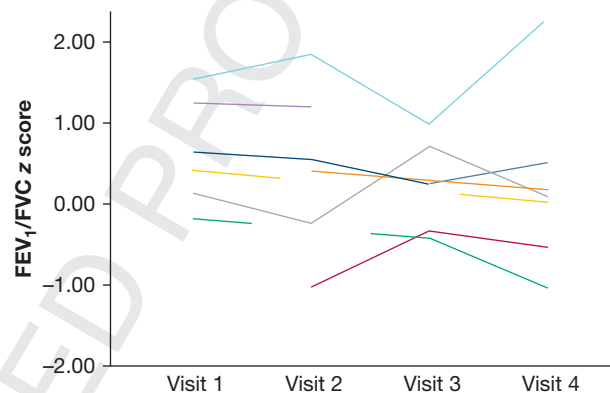
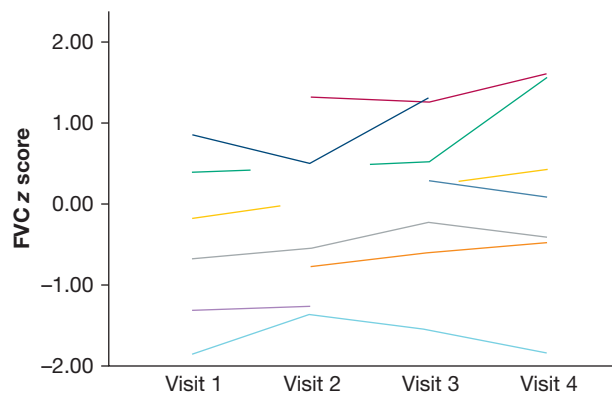
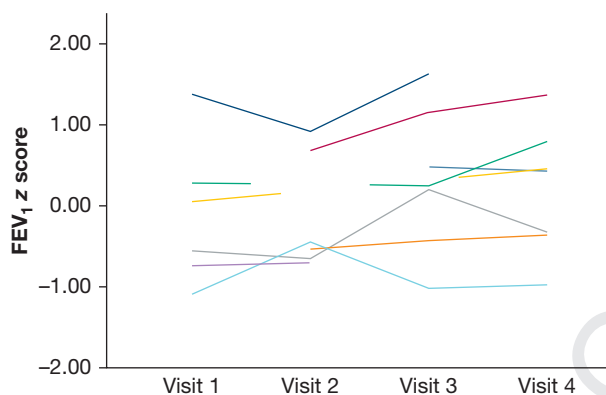


Figure 6 – Boxplots of xenon gas transfer ratios from patients at visits 1 to 4 as well as metrics from an age- and sex-matched healthy cohort. M = membrane. Open circles denote data > 1.5 interquartile range; star denotes data > 3 interquartile range.

imaging and ventilation, with six of eight patients outside the median \pm IQR of normal age- and sex-matched patients at 51 weeks.

Several studies have reported reduced gas transfer to the RBC in patients hospitalized due to COVID-19.²¹⁻²³ Because xenon gas transfer depends on both the xenon



— Patient 1 — Patient 2 — Patient 3 — Patient 4 — Patient 5 — Patient 6 — Patient 7 — Patient 8 — Patient 9

Figure 7 – Spaghetti plots of FEV_1 z score, FVC z score, FEV_1/FVC z score, K_{CO} z score, and TL_{CO} z score. K_{CO} = carbon monoxide transfer coefficient; TL_{CO} = gas transfer test.

uptake in the lung tissue and the xenon uptake in the RBCs, a combination of lung perfusion abnormalities and/or alveolar/interstitial endothelial changes may be mechanistically driving the reduced xenon gas transfer seen in patients following COVID-19. Although not directly comparable to the results from those studies due to differences in imaging parameters, our findings are in accordance with the reporting of significantly lower RBC:M values between hospital discharge and 24 weeks'

postdischarge in previous studies.²⁰⁻²² In the current study, the inclusion of data from age- and sex-matched healthy control subjects shows that these changes are not due to age or sex differences between control subjects and patients in this study. RBC:gas and M:gas did not show significant longitudinal change once adjusted for multiple comparisons, implying that the change in RBC:M was a combined effect of changes in both M and RBC. A significant reduction in $M T_2^*$ at visit 2 was also

1431 **TABLE 3]** Effect of Pulmonary Blood Volume, Pulmonary Blood Flow, Mean Transit Time, VDP, and TL_{CO} z Score on
 1432 RBC:M Tested Using Linear Mixed-Effect Model Analysis With a Random Intercept

	Estimated Coefficient	P Value	Lower CI	Upper CI
Pulmonary blood volume (mL/100 mL)	0.0016	.002	0.0007	0.0025
Pulmonary blood flow (mL/100 mL/min)	0.00067	.015	0.00014	0.00120
Mean transit time (s)	0.0082	.076	-0.00093	0.01729
VDP (%)	-0.025	.009	-0.0427	-0.007
TL _{CO} z score	0.048	< .001	0.027	0.069

1440 The estimated coefficients of the models, *P* values, and CIs are shown in the table. M = membrane; TL_{CO} = gas transfer test; VDP = ventilation defect
 1441 percentage.

1442
 1443 found. The physiological mechanisms behind changes in
 1444 M T₂* are not well established and are discussed further
 1445 in the [online supplement](#).

1446
 1447 We also found that changes in xenon gas transfer
 1448 increased significantly with increased TL_{CO} z score,
 1449 VDP, and lung perfusion metrics (pulmonary blood
 1450 volume and pulmonary blood flow). All patients with
 1451 DCE data available displayed an increase in regional
 1452 pulmonary blood flow and volume between visits 1 and
 1453 2, despite only one having a substantial perfusion defect.
 1454 This may indicate microvascular improvements at
 1455 12 weeks, and that microvascular recovery may be
 1456 partially driving changes in RBC:M in these patients. In
 1457 parallel, a concomitant reduction in M signal due to
 1458 resolution of postinfection endothelial inflammation
 1459 could contribute to the increase in RBC:M with time.

1460
 1461 Although we see global correlations between RBC:M,
 1462 ventilation, and perfusion, regional heterogeneity in
 1463 RBC:M did not visually agree with ventilation or
 1464 perfusion heterogeneity; for example, as shown in
 1465 [Figure 3](#), Patient 8 has a visually heterogeneous RBC:M
 1466 map but no visual concordance with pulmonary blood
 1467 flow heterogeneity and homogeneous ventilation on the
 1468 similar slices presented. Further work assessing regional
 1469 distributions seen in the different functional MR images
 1470 available here is warranted to evaluate regional
 1471 correlations quantitatively.

1472
 1473 In this study, most patients (seven of nine) did not
 1474 report significant breathlessness at visit 2 (12 weeks),
 1475 despite lower RBC:M than the control reference data.
 1476 The two patients who reported breathlessness at visit 2
 1477 had the two lowest RBC:M values at that visit. Larger
 1478 studies in symptomatic patients are needed to further
 1479 investigate links between RBC:M and breathlessness or
 1480 other post-COVID-19 symptoms. Fully recovered post-
 1481 COVID-19 control groups will be important in further
 1482 studies investigating post-COVID-19 breathlessness
 1483 with these imaging techniques.

1484
 1485 Median patient ADC and Lm_D were within the age- and
 1486 sex-matched reference range at visits 1 and 2,³⁵ with no
 1487 significant change at visit 2, indicating that airway
 1488 dimensions were not increased in these nine patients
 1489 who had COVID-19 but no signs of interstitial lung
 1490 damage on structural imaging. This study excluded
 1491 patients with signs of interstitial lung damage, as
 1492 previous work has shown that patients with interstitial
 1493 lung diseases can have reduced xenon gas transfer,⁶
 1494 alterations in lung microstructure measured using ¹²⁹Xe
 1495 MRI,⁶ reductions in lung ventilation,⁴⁶ and reductions in
 1496 lung perfusion.⁴⁷ Although this means that there is
 1497 considerable promise for lung MRI to provide
 1498 longitudinal biomarkers in patients with signs of
 1499 interstitial lung damage, it also suggests that persistent
 1500 perfusion, ventilation, gas transfer, and lung
 1501 microstructure abnormalities may be mechanistically
 1502 related to the visible tissue changes within a cohort with
 1503 structural lung abnormalities. Further work using a ¹H
 1504 and ¹²⁹Xe protocol in patients with established
 1505 pulmonary fibrosis due to COVID-19 on CT scan
 1506 imaging is the subject of an ongoing study (UKILD).²⁹

1507
 1508 Minor ventilation heterogeneity and defects were
 1509 present in this cohort shortly following acute illness;
 1510 these defects improved over time, which is consistent
 1511 with the findings of Grist et al²¹ and of Li et al.²⁰ Overall,
 1512 the current study and the findings from previous
 1513 literature suggest it is unlikely that impaired lung
 1514 ventilation is the primary cause of ongoing symptoms
 1515 following the acute stage of COVID-19 and that the
 1516 pathophysiology is not primarily of the airways.

1517
 1518 The main limitation of the current study is the limited
 1519 number of participants, which was largely caused by the
 1520 challenging nature of recruiting patients for scanning
 1521 directly following a recent hospitalization due to
 1522 COVID-19 in the first wave of the pandemic. In
 1523 addition, not all patients had DCE lung perfusion
 1524 imaging or PFTs at all examinations (due to

1541 aerosolization constraints). The numbers recruited limit
 1542 correlations with symptoms, activity, and lung function,
 1543^{Q16} as well as the statistical tests used to test for change. All
 1544 ¹²⁹Xe acquisitions were acquired at FRC plus 1 L,
 1545 resulting in some variability between patients in the lung
 1546 inflation state. A final potential source of bias in this
 1547 study is that five patients who were potentially eligible
 1548 for the study were excluded due to chest size exceeding
 1549 the size of the xenon MRI coil.
 1550

1551 Interpretation

1552 This study found that in a cohort of patients who were
 1553 hospitalized with COVID-19 pneumonia of moderate
 1554 severity who had normal CT scan/lung structural
 1555 imaging, ¹²⁹Xe gas transfer improved at 12 weeks but did
 1556 not return to within a normal range within 1 year
 1557 following hospitalization. Improvements in ¹²⁹Xe gas
 1558 transfer were associated with an increased lung
 1559 perfusion on DCE-MRI and increased TL_{CO} z score;
 1560 therefore, abnormalities in ¹²⁹Xe gas transfer may be a
 1561 marker of ongoing microvascular abnormalities post-
 1562 COVID-19.
 1563

1564 TL_{CO} z score was within a normal range for seven of
 1565 eight patients with available data at 51 weeks'
 1566 posthospitalization. This indicates that ¹²⁹Xe gas transfer
 1567 may be a more sensitive measure of gas exchange in this
 1568 population and that it may be able to identify
 1569 abnormalities that routine clinical tests overlook.
 1570

1571 We believe this to be the first follow-up study of similar
 1572 patients with such an extensive range of functional lung
 1573 imaging techniques. Our findings show the sensitivity
 1574 and complementary nature of functional MRI to follow-
 1575 up post-COVID-19 lung pathophysiology in a clinical
 1576 setting.
 1577

1580^{Q17} Q18 Funding/Support

1581 This study was supported by a Medical Research
 1582 Council grant [MR/M008894/1]; GSK and GE for
 1583 investigator led grant funding; BHF Intermediate
 1584 Clinical Fellowship (FS/18/13/33281); and JMW Medical
 1585 Research Council grant ["Expansion of state-of-the-art
 1586 MR imaging infrastructure for pulmonary disease
 1587 stratification: POLARIS," MR/M008894/1]. A. A. R. T.
 1588 was supported by a British Heart Foundation
 1589^{Q17} Intermediate Clinical Fellowship [FS/18/13/33281].
 1590
 1591
 1592
 1593
 1594
 1595

Financial/Nonfinancial Disclosures

1596^{Q18} The authors have reported to CHEST the following
 1597 disclosures. The following authors have declarations of
 1598 support from organizations for the submitted work: P. J.
 1599 C. H. receives grant funding from GSK and Bayer. A. A.
 1600 R. T. is funded by British Heart Foundation
 1601 Intermediate Clinical Fellowship and grant funding
 1602 from Janssen-Cilag Ltd. A. L. receives grant funding
 1603 from the British Heart Foundation (fellowship award).
 1604 G. J. receives grant funding from AstraZeneca, Biogen,
 1605 Galecto, GSK, RedX, Pliant, and Genentech. A. J. S.
 1606 receives grant funding from the National Institute for
 1607 Health and Care Research (NIHR) (AI award),
 1608 Wellcome (Innovator award), and Janssen-Cilag Ltd
 1609 (project grant). J. M. W. receives grant funding from the
 1610 Medical Research Council, GSK (investigator led
 1611 research grant), and GE Healthcare. F. G. receives grant
 1612 or contract funding from Oxford NIHR Biomedical
 1613 Research Centre, NIHR (EXPLAIN trial), POLAREAN
 1614 Ltd, and GE Healthcare. K. M. J. has received National
 1615 Institutes of Health grant funding for the development
 1616 of an MRI sequence used in this work. The following
 1617 authors declare financial relationships with
 1618 organizations that might have an interest in the
 1619 submitted work in the previous 3 years: A. C. is an
 1620 employee of GSK. F. J. W. was an employee of GSK at
 1621 the time of the study. A. C. is a shareholder in GSK. F. J.
 1622 was a shareholder in GSK at the time of the study. R. F. S.
 1623 is employed by, and a shareholder of, GE Healthcare. A.
 1624 L. receives funding support from Janssen-Cilag Ltd for
 1625 meetings/travel. A. A. R. T. receives funding from
 1626 Janssen-Cilag Ltd for meetings/travel. G. J. receives
 1627 consulting fees from Bristol Myers Squibb, Daewoong,
 1628 Veracyte, Resolution Therapeutics, RedX, Pliant, and
 1629 Chiesi. A. J. S. receives consultancy fees from Janssen-
 1630 Cilag Ltd. G. J. receives payment from Chiesi, Roche,
 1631 patientMpower, AstraZeneca, GSK, and Boehringer
 1632 Ingelheim for lectures. A. J. S. receives payment from
 1633 Janssen-Cilag Ltd. F. G. receives payment from
 1634 POLAREAN Ltd. G. J. is a trustee of Action for
 1635 Pulmonary Fibrosis. F. G. is the president of the
 1636 European Society for Thoracic Imaging. None declared
 1637 (L. C. S., G. J. C., H.-F. C., L. J. S., J. W., J. M., Z. G., T.
 1638 N., M. P., J. A. E., S. T., S. S., L. G., H. M., J. B., D. J. C., L.
 1639 A., J. R., M. B., A. M. B., G. N., O. R., M. R. R., R. M., N.
 1640 J. S., J. G., S. R., G. H. M., R. L., P. J. C.).
 1641
 1642
 1643
 1644
 1645
 1646
 1647
 1648
 1649
 1650

1651 Acknowledgments

1652 **Author contributions:** J. M. W. and L. C. S.
1653 had full access to all the data in the study and
1654 take responsibility for the integrity of the data
1655 and the accuracy of the data analysis. J. M.
1656 W., A. A. R. T., R. L., P. J. C., G. H. M., A. C.,
1657 F. J. W., K. M. J., R. F. S., F. G., G. J., A. L., J.
1658 G., and G. J. C. conceived and designed the
1659 study. L. C. S., G. J. C., H. F. C., P. J. C. H., L.
1660 J. S., J. W., J. M., Z. G., T. N., M. P., P. W., J.
1661 A. E., J. B., S. T., S. S., L. G., H. M., D. J. C., L.
1662 A., J. R., M. B., A. M. B., M. R. R., G. N., O.
1663 R., R. M., J. E. B., N. J. S., A. J. W., S. R., and
1664 L. W. obtained, prepared, and analyzed the
1665 data. L. C. S. wrote the first draft. All authors
1666 assume responsibility for the overall content
1667 and integrity of the article. All authors were
1668 involved in reviewing and shaping the
1669 manuscript, and all approved the final
1670 version prior to submission.

1667 **Role of sponsors:** The sponsor had no role in
1668 the design of the study, the collection and
1669 analysis of the data, or the preparation of the
1670 manuscript.

1670 **Additional information:** The e-Figures and
1671 e-Tables are available online under
1672 "Supplementary Data."

1673 References

- 1675 1. Lang M, Som A, Carey D, et al.
1676 Pulmonary vascular manifestations of
1677 COVID-19 pneumonia. *Radiol
Cardiothorac Imaging*. 2020;2(3):e200277.
- 1678 2. Loo J, Spittle DA, Newnham M. COVID-
1679 19, immunothrombosis and venous
1680 thromboembolism: biological
1681 mechanisms. *Thorax*. 2021;76(4):412-420.
- 1682 3. Attaway AH, Scheraga RG, Bhimraj A,
1683 Biehl M, Hatipoglu U. Severe Covid-19
1684 pneumonia: pathogenesis and clinical
1685 management. *BMJ*. 2021;372:n436.
- 1686 4. Robey RC, Kemp K, Hayton P, et al.
1687 Pulmonary sequelae at 4 months after
1688 COVID-19 infection: a single-centre
1689 experience of a COVID follow-up service.
1690 *Adv Ther*. 2021;38(8):4505-4519.
- 1691 5. Stewart NJ, Smith LJ, Chan HF, et al. Lung
1692 MRI with hyperpolarised gases: current &
1693 future clinical perspectives. *Br J Radiol*.
1694 2022;95(1132):20210207.
- 1695 6. Collier GJ, Eaden JA, Hughes PJ, et al.
1696 Dissolved (129) Xe lung MRI with four-
1697 echo 3D radial spectroscopic imaging:
1698 quantification of regional gas transfer in
1699 idiopathic pulmonary fibrosis. *Magn
Reson Med*. 2021;85(5):2622-2633.
- 1700 7. Wielputz MO, Puderbach M, Kopp-
1701 Schneider A, et al. Magnetic resonance
1702 imaging detects changes in structure and
1703 perfusion, and response to therapy in
1704 early cystic fibrosis lung disease. *Am J
Respir Crit Care Med*. 2014;189(8):
1705 956-965.
- 1706 8. Ohno Y, Koyama H, Matsumoto K, et al.
1707 Dynamic MR perfusion imaging:
1708 capability for quantitative assessment of
1709 disease extent and prediction of outcome
1710 for patients with acute pulmonary
1711 thromboembolism. *J Magn Reson
Imaging*. 2010;31(5):1081-1090.
- 1712 9. Thomen RP, Walkup LL, Roach DJ, et al.
1713 Regional structure-function in cystic
1714 fibrosis lung disease using hyperpolarized
1715 (129)Xe and ultrashort echo magnetic
1716 resonance imaging. *Am J Respir Crit Care
Med*. 2020;202(2):290-292.
- 1717 10. Tafti S, Garrison WJ, Mugler JP 3rd, et al.
1718 Emphysema index based on
1719 hyperpolarized (3)He or (129)Xe diffusion
1720 MRI: performance and comparison with
1721 quantitative CT and pulmonary function
1722 tests. *Radiology*. 2020;297(1):201-210.
- 1723 11. McIntosh MJ, Kooner HK, Eddy RL, et al.
1724 CT mucus score and 129Xe MRI
1725 ventilation defects after 2.5-years anti-IL-
1726 5R α in eosinophilic asthma [published
1727 online ahead of print February 11, 2023].
1728 *Chest*. [https://doi.org/10.1016/j.chest.2023.
02.009](https://doi.org/10.1016/j.chest.2023.02.009)
- 1729 12. Kaushik SS, Cleveland ZI, Cofer GP, et al.
1730 Diffusion-weighted hyperpolarized Xe-
1731 129 MRI in healthy volunteers and
1732 subjects with chronic obstructive
1733 pulmonary disease. *Magn Reson Med*.
1734 2011;65(4):1155-1165.
- 1735 13. Chan HF, Weatherley ND, Johns CS, et al.
1736 Airway microstructure in idiopathic
1737 pulmonary fibrosis: assessment at
1738 hyperpolarized He-3 diffusion-weighted
1739 MRI. *Radiology*. 2019;291(1):223-229.
- 1740 14. Marshall H, Stewart NJ, Chan HF, Rao M,
1741 Norquay G, Wild JM. In vivo methods
1742 and applications of xenon-129 magnetic
1743 resonance. *Prog Nucl Magn Reson
Spectrosc*. 2021;122:42-62.
- 1744 15. Wang ZY, Rankine L, Bier EA, et al. Using
1745 hyperpolarized Xe-129 gas-exchange MRI
1746 to model the regional airspace, membrane,
1747 and capillary contributions to diffusing
1748 capacity. *J Appl Physiol*. 2021;130(5):
1749 1398-1409.
- 1750 16. Weatherley ND, Stewart NJ, Chan HF,
1751 et al. Hyperpolarised xenon magnetic
1752 resonance spectroscopy for the
1753 longitudinal assessment of changes in gas
1754 diffusion in IPF. *Thorax*. 2019;74(5):
1755 500-502.
- 1756 17. Wang JM, Robertson SH, Wang Z, et al.
1757 Using hyperpolarized (129)Xe MRI to
1758 quantify regional gas transfer in idiopathic
1759 pulmonary fibrosis. *Thorax*. 2018;73(1):
1760 21-28.
- 1761 18. Myc L, Qing K, He M, et al.
1762 Characterisation of gas exchange in
1763 COPD with dissolved-phase
1764 hyperpolarised xenon-129 MRI. *Thorax*.
1765 2021;76(2):178-181.
- 1766 19. Wang Z, Robertson SH, Wang J, et al.
1767 Quantitative analysis of hyperpolarized
1768 (129) Xe gas transfer MRI. *Med Phys*.
1769 2017;44(6):2415-2428.
- 1770 20. Li H, Zhao X, Wang Y, et al. Damaged
1771 lung gas exchange function of discharged
1772 COVID-19 patients detected by
1773 hyperpolarized (129)Xe MRI. *Sci Adv*.
1774 2021;7(1).
- 1775 21. Grist JT, Chen M, Collier GJ, et al.
1776 Hyperpolarized (129)Xe MRI
1777 abnormalities in dyspneic patients
1778 3 months after COVID-19 pneumonia:
1779 preliminary results. *Radiology*.
1780 2021;301(1):E353-E360.
- 1781 22. Grist JT, Collier GJ, Walters H, et al. Lung
1782 abnormalities depicted with
1783 hyperpolarized xenon MRI in patients
1784 with long COVID. *Radiology*. 2022;220069.
1785 1708
- 1786 23. Matheson AM, McIntosh MJ, Kooner HK,
1787 et al. Persistent (129)Xe MRI pulmonary
1788 and CT vascular abnormalities in
1789 symptomatic individuals with post-acute
1790 COVID-19 syndrome. *Radiology*.
1791 2022;220492. 1713
- 1792 24. Wild JM, Collier G. (129)Xe Pulmonary
1793 MRI for individuals with post-acute
1794 COVID-19 syndrome. *Radiology*.
1795 2022;221361. 1714
- 1796 25. Yang S, Zhang Y, Shen J, et al. Clinical
1797 potential of UTE-MRI for assessing
1798 COVID-19: patient- and lesion-based
1799 comparative analysis. *J Magn Reson
Imaging*. 2020;52(2):397-406. 1720
- 1800 26. Johns CS, Swift AJ, Rajaram S, et al. Lung
1801 perfusion: MRI vs. SPECT for screening in
1802 suspected chronic thromboembolic
1803 pulmonary hypertension. *J Magn Reson
Imaging*. 2017;46(6):1693-1697. 1721
- 1804 27. Rysz S, Al-Saadi J, Sjostrom A, et al.
1805 COVID-19 pathophysiology may be
1806 driven by an imbalance in the renin-
1807 angiotensin-aldosterone system. *Nat
Commun*. 2021;12(1):2417. 1722
- 1808 28. Yu JZ, Granberg T, Shams R, et al. Lung
1809 perfusion disturbances in nonhospitalized
1810 post-COVID with dyspnea—a magnetic
1811 resonance imaging feasibility study.
1812 *J Intern Med*. 2022;292(6):941-956. 1723
- 1813 29. Wild JM, Porter JC, Molyneux PL, et al.
1814 Understanding the burden of interstitial
1815 lung disease post-COVID-19: the UK
1816 Interstitial Lung Disease-Long COVID
1817 Study (UKILD-Long COVID). *BMJ Open
Respir Res*. 2021;8(1). 1724
- 1818 30. Stanojevic S, Graham BL, Cooper BG,
1819 et al. Official ERS technical standards:
1820 Global Lung Function Initiative reference
1821 values for the carbon monoxide transfer
1822 factor for Caucasians. *Eur Respir J*.
1823 2017;50(3). 1725
- 1824 31. Quanjer PH, Stanojevic S, Cole TJ, et al.
1825 Multi-ethnic reference values for
1826 spirometry for the 3-95-yr age range: the
1827 Global Lung Function 2012 equations. *Eur
Respir J*. 2012;40(6):1324-1343. 1726
- 1828 32. Norquay G, Collier GJ, Rao M, Stewart NJ,
1829 Wild JM. (129)Xe-Rb spin-exchange
1830 optical pumping with high photon
1831 efficiency. *Phys Rev Lett*. 2018;121(15):
1832 153201. 1727
- 1833 33. Smith LJ, Horsley A, Bray J, et al. The
1834 assessment of short- and long-term
1835 changes in lung function in cystic fibrosis
1836 using Xe-129 MRI. *Eur Respir J*.
1837 2020;56(6). 1728
- 1838 34. Stewart NJ, Norquay G, Griffiths PD,
1839 Wild JM. Feasibility of human lung
1840 ventilation imaging using highly polarized
1841 naturally abundant xenon and optimized
1842 three-dimensional steady-state free
1843 precession. *Magn Reson Med*. 2015;74(2):
1844 346-352. 1729
- 1845 35. Chan HF, Stewart NJ, Norquay G,
1846 Collier GJ, Wild JM. 3D diffusion-
1847 weighted (129) Xe MRI for whole lung
1848 1760

- 1761 morphometry. *Magn Reson Med.* 2018;79(6):2986-2995.
- 1762
- 1763 36. Johnson KM, Fain SB, Schiebler ML, Nagle S. Optimized 3D ultrashort echo time pulmonary MRI. *Magn Reson Med.* 2013;70(5):1241-1250.
- 1764
- 1765
- 1766 37. Li KL, Zhu XP, Waterton J, Jackson A. Improved 3D quantitative mapping of blood volume and endothelial permeability in brain tumors. *J Magn Reson Imaging.* 2000;12(2):347-357.
- 1767
- 1768
- 1769
- 1770 38. Cheng HL, Wright GA. Rapid high-resolution T(1) mapping by variable flip angles: accurate and precise measurements in the presence of radiofrequency field inhomogeneity. *Magn Reson Med.* 2006;55(3):566-574.
- 1771
- 1772
- 1773
- 1774 39. Chan HF, Collier GJ, Parra-Robles J, Wild JM. Finite element simulations of hyperpolarized gas DWI in micro-CT meshes of acinar airways: validating the cylinder and stretched exponential models of lung microstructural length scales. *Magn Reson Med.* 2021;86(1):514-525.
- 1775
- 1776 40. Chatfield M, Mander A. The Skillings-Mack test (Friedman test when there are missing data). *Stata J.* 2009;9(2):299-305.
- 1777
- 1778 41. Benjamini Y, Hochberg Y. Controlling the false discovery rate: a practical and powerful approach to multiple testing. *J R Stat Soc Series B Stat Methodol.* 1995;57(1):289-300.
42. Team RC. R: A language and environment for statistical computing. *MSOR connections.* 2014;1.
43. Petersson-Sjogren M, Chan HF, Collier GJ, et al. Airspace dimension assessment (AiDA) by inhaled nanoparticles: benchmarking with hyperpolarised (129)Xe diffusion-weighted lung MRI. *Sci Rep.* 2021;11(1):4721.
44. Knight SR, Ho A, Pius R, et al. Risk stratification of patients admitted to hospital with covid-19 using the ISARIC WHO Clinical Characterisation Protocol: development and validation of the 4C Mortality Score. *BMJ.* 2020;370:m3339.
45. Williams B. Evaluation of the utility of NEWS2 during the COVID-19 pandemic. *Clin Med (Lond).* 2022;22(6):539-543.
46. Tibiletti M, Eaden JA, Naish JH, et al. Imaging biomarkers of lung ventilation in interstitial lung disease from (129)Xe and oxygen enhanced (1)H MRI. *Magn Reson Imaging.* 2023;95:39-49.
47. Weatherley ND, Eaden JA, Hughes PJC, et al. Quantification of pulmonary perfusion in idiopathic pulmonary fibrosis with first pass dynamic contrast-enhanced perfusion MRI. *Thorax.* 2021;76(2):144-151.